Acta Materialia 142 (2018) 95–106

Contents lists available at ScienceDirect

Acta Materialia

journal homepage: www.elsevier.com/locate/actamat

Full length article

On the microstructural origins of martensitic transformation arrest in a NiCoMnIn magnetic shape memory alloy

N.M. Bruno [a], D. Salas [a], S. Wang [a], Igor V. Roshchin [a], R. Santamarta [b], R. Arroyave [a], T. Duong [a], Y.I. Chumlyakov [c], I. Karaman [a, *]

[a] Department of Materials Science and Engineering, Texas A&M University, College Station, TX, 77845, USA
[b] Departament de Fisica, Universitat de les Illes Balears, Palma de Mallorca, E-07122, Spain
[c] Siberian Physical Technical Institute, Tomsk State University, Tomsk, 634050, Russia

ARTICLE INFO

Article history:
Received 3 July 2017
Received in revised form
17 August 2017
Accepted 18 August 2017
Available online 19 August 2017

Keywords:
Magnetic shape memory alloys
Martensitic transformation
Transformation arrest
NiCoMnIn
Crystallographic ordering

ABSTRACT

The martensitic transformation arrest phenomenon in $Ni_{45}Co_5Mn_{36.6}In_{13.4}$ meta-magnetic shape memory alloy (MMSMA) single crystals was investigated as a function of secondary annealing heat treatments, using thermo-magnetometry and transmission electron microscopy (TEM). Dark-field images of the austenite phase at room temperature revealed the long range $L2_1$ and B2 ordered microstructural landscape with different morphologies in the annealed single crystals. Their measured thermomagnetic responses demonstrated full transformation arrest after certain heat treatments and unique microstructural morphologies. Martensitic transformation hysteresis, range, and enthalpy were measured in the annealed partially- or non-arrested single crystals. With the data, herein, we found that the samples with long range $L2_1$ ordering exhibit martensitic transformation at higher temperatures than some of the crystals of the same composition showing predominantly B2 order. This finding opposes the previous reports on the effect of annealing on the martensitic transformation characteristics of MMSMAs. We provide evidence that long range order promoted with high temperature annealing is not the only microstructural feature capable of influencing the martensitic transition in NiCoMnIn MMSMAs. Data suggests that quenched in vacancies, in addition to long range order, also influence the transformation characteristics.

1. Introduction

1.1. Overview

Meta-magnetic shape memory alloys (MMSMAs) are a recently discovered class of active materials that exhibit reversible martensitic transformations. The martensitically transforming phases of these alloys have very different magnetic ordering (i.e. ferromagnetic austenite and anti-ferromagnetic martensite or vice-versa). They can potentially be useful as functional components in magneto-thermo-mechanical systems [1–13] since martensitic transformations can be driven by magnetic field [14], mechanical stress [15], or various degrees of under- (over-) cooling (heating). The magneto-thermo-mechanical response of MMSMAs are tailorable through microstructural changes [5,9,10,16–18], rather than only through compositional modifications [19], sometimes just with simple heat treatments; thus, a single composition can be suitable for a variety of engineering applications.

Over the last decade, it has been shown that NiMnX (X = In, Ga, Sn, Sb, Al) MMSMAs demonstrate a wide range of unusual properties due to the strong magneto-structural, thermo-mechanical, and magneto-thermal coupling. These include, but are not limited to, magnetization reversal through magnetic field driven martensite reorientation [20–25], thermal energy generation and absorption via reversible phase transformation latent heat [19,26], magnetic-field induced martensitic transformation coupled to large reversible macroscopic shape change [1,6,27], magnetic exchange bias effects [28,29], and giant magnetoresistance [30].

More recently, it has been discovered that $Ni_{45}Co_5Mn_{36.6}In_{13.4}$ (at. %) [8], $Ni_{50}Mn_{34}In_{16}$ (Fe, Cr) [31], $Ni_{43}Co_{12}Mn_{20}Ga_{25}$ [32] and $Ni_{50-x}Co_xMn_{39}Sn_{11}$ (x = 7, 9) [33] MMSMAs can be microstructurally engineered, through secondary heat treatments, microstructural defect generation, and crystallographic ordering,

* Corresponding author.
E-mail address: ikaraman@tamu.edu (I. Karaman).

https://doi.org/10.1016/j.actamat.2017.08.037
1359-6454/

into magnetic and structural glasses [8,33,34]. It is believed that there are intricate relationships between these microstructural factors (such as intrinsic long-range ordering and anti-site defects), martensitic transformation, and structural and magnetic, time-dependent glassy behaviors that result in unprecedented multi-functional behaviors in these materials. Interestingly, the glassy behaviors in MMSMAs almost always coincide with the suppression or partial arrest of martensitic transformations. However, the nature of the relationships between the microstructure and the change in martensitic transformation characteristics, and the microstructural origins of transformation arrest as a function of various magneto-thermo-mechanical loading schemes, have not been yet clearly revealed. Below, we first introduce a few relevant basics in MMSMAs that will help in understanding the possible microstructural features that may play a role in the aforementioned behaviors and the concept of martensitic transformation arrest. A NiCoMnIn MMSMA is selected as the model material system, as opposed to NiCoMnSn [10] or NiCoMnGa [35], due to the high level of sensitivity of its transformation characteristics and magnetic behavior to microstructural changes.

1.2. Crystal ordering and transformation behavior in MMSMAs

In the ternary, or Co-containing quaternary, Ni(Co)MnIn MMSMAs, the austenite phase is normally characterized by a cubic superstructure (Heusler type) and exhibits either ferromagnetic or paramagnetic behaviors [36]. On cooling, the austenite phase transforms into the martensite phase by a diffusionless first-order phase transformation through a set of critical temperatures, namely martensite start (finish), M_s (M_f) temperatures. The martensite thus inherits the nearest neighbor and next-nearest neighbor atomic species from the austenite phase. During the transformation, the atoms at the austenite lattice sites collectively shift a fraction of interatomic distances along the austenite habit plane. The martensite phase exhibits a lower degree of crystal symmetry than the austenite phase and different magnetic ordering through distance-dependent (Ruderman-Kittel-Kasuya-Yosida) RKKY-type interactions between the magnetic species, in particular between Mn and Co atoms [37,38].

The ferromagnetic phase in MMSMAs can be stabilized by an applied magnetic field. In the case of NiCoMnIn, this is often the austenite phase, but in other MMSMAs including FeMnGa [39,40], NiMnGa [41–43], CoMnGe(Fe) [44], the martensite phase is ferromagnetic and austenite can be paramagnetic. The applied magnetic field tends to lower the free energy of the ferromagnetic phase, and therefore, stabilizes the phase over a broader temperature range. This effect is observed as a decrease in M_s with magnetic field in NiCoMnIn alloys as depicted in Fig. 1.

In Fig. 1, two thermomagnetic field-cooling and field-heating curves are shown as an example of a meta-magnetic transition. The right-most curves are measured under a low magnetic field, 1 T, and the leftmost curves under 7 T. On cooling from 400 K, the MMSMA undergoes a structural transition from austenite to martensite with sufficient undercooling, and therefore loses the magnetic properties of the ferromagnetic austenite. On subsequent field-heating, the alloy transforms back to the austenite phase starting at A_s, the austenite start temperature, and finishing at the A_f, or austenite finish temperature. Applying a larger magnetic field to the MMSMA results in a decrease in all martensitic transformation temperatures as shown in Fig. 1. Applying an even larger magnetic field has been shown to further decrease the M_s temperature until the transformation becomes fully arrested [45,46].

There are also other ways to decrease the M_s temperature and

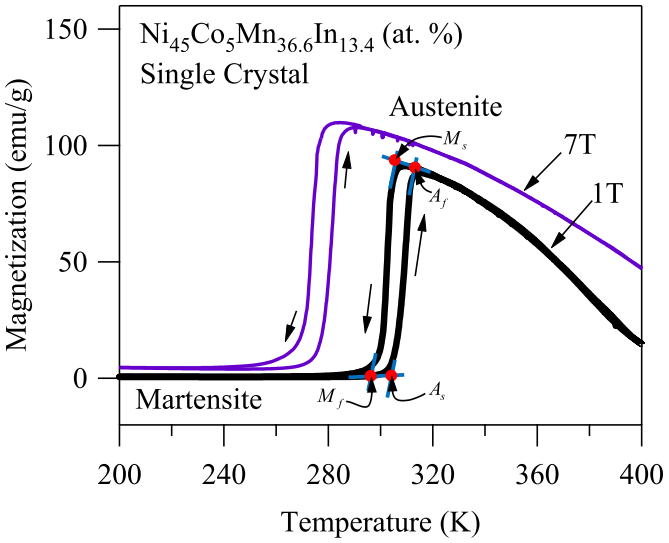

Fig. 1. Thermomagnetic field-cooling and field-heating responses of $Ni_{45}Co_5Mn_{36.6}In_{13.4}$ (at.%) MMSMA single crystals under 1 T and 7 T. The high temperature austenite phase is stabilized by increased applied magnetic fields as shown by a decrease in the M_s temperature and increase in saturation magnetization. Applying larger magnetic fields will lead to further decreases in M_s and eventually to the suppression of the martensitic transformation.

prevent austenite from transforming to martensite (causing the transformation arrest). For instance, it has recently been discovered that the crystal site occupancy or long-range order in NiCoMnIn austenite alters the transformation behavior (that shown in Fig. 1) and influences the M_s temperature through magneto-structural coupling [8,18,47]. The defect-free superstructure, shown in Fig. 2 for the stoichiometric composition $(Ni,Co)_2MnIn$, is capable of exhibiting B2 (Fig. 2a) and $L2_1$ (Fig. 2b) long range ordering from simple diffusion-promoting annealing treatments above and below the order-disorder (ODO) temperature, respectively [48]. Anti-site defects and vacancies resulting from any solution heat treatment are often ignored in reports describing long range order in these alloys. Nonetheless, long range order, vacancy concentration, and anti-site defects all influence the interatomic distance of the magnetic species, Co and Mn. Thus, as a result, the magneto-structural coupling is expected to vary within the crystal lattice following the RKKY-type interactions, and lead to different magneto-structural behavior for a single composition alloy depending on the degree of order.

In particular, each of the differently ordered austenite phases are expected to exhibit different bulk magnetic properties, lattice parameters, and configurational entropy. These resulting properties influence many of the transformation characteristics including the transformation temperatures, thermal hysteresis, thermal transition range, and the change in magnetic Zeeman energy across the transformation. Moreover, each ordered phase should have different sensitivities to vacancy concentration and microstructural defects including dislocations [49], which would further influence the transformation characteristics. In addition, an increase in the degree of long range order, defined as the fraction of $L2_1$ phase in the austenite, is believed to lead to a decrease in M_s and eventually, the suppression of the thermo-elastic martensitic transformation. In an attempt to understand the origins of this suppression and transformation arrest in these alloys, below we give a brief critical account of various reported physical behaviors and posit that the microstructural features, that will be introduced herein, may play a

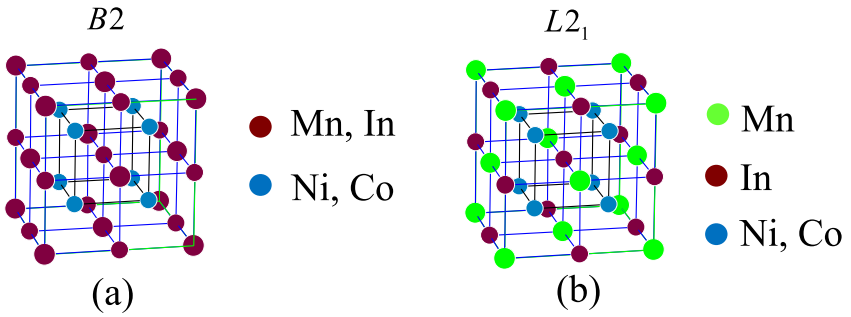

Fig. 2. The crystal structure of the $(Ni,Co)_2MnIn$ compound with B2 ordering (a) and $L2_1$ ordering (b).

defining role.

1.3. Thermodynamic and kinetic transformation arrest

There have been different reports of transformation arrest in MMSMAs and to better understand the influence of microstructural features that drive these behaviors, they are briefly mentioned below. To begin with, suppression of martensitic transformation has been explained from both thermodynamic and kinetic perspectives [50] and the microstructure in MMSMAs is also well-known to influence the kinetics and thermodynamics of the martensitic transformation. MMSMAs that exhibit arrested transformations have also been shown to exhibit non-ergodic glass-like behaviors [8,33,34]. We therefore ask and aim to answer "What microstructural features will generate this behavior in NiCoMnIn MMSMAs?"

There has been much debate in the literature regarding which aspect, kinetics or thermodynamics, plays a more dominant role in the transformation arrest. This is because the arrest appears to exhibit a dependency on both at low temperatures. As a solution, Xu et al. [50] proposed to generally rename "kinetic arrest" and "thermodynamic arrest" to "thermal transformation arrest" in an attempt encompass both, thermodynamic and kinetic implications.

Thermodynamic arrest is said to take place in field-cooling experiments like those shown in Fig. 1. At some critical temperature and field-level, the magnetic entropy difference between the austenite and martensite phases is believed to overcome the vibrational entropy difference between the two phases, and thus the total difference in their entropy becomes zero, $\Delta S_{tr}^{A\rightarrow M} = S_{Total}^{M} - S_{Total}^{A} = 0$. The thermodynamic driving force, i.e. $\Delta G = \Delta S_{tr}^{A\rightarrow M} \cdot \Delta T$ (where ΔT is undercooling) at the transformation temperature, becomes zero and the transformation cannot initiate, i.e. martensite will not nucleate, with any degree of undercooling [50]. The balance between the magnetic and vibrational entropy contributions can also be affected by long range crystal ordering, as mentioned in the previous section. For instance, the total entropy, S_{Total}, of martensite or austenite is defined by the superposition of configurational, vibrational, magnetic, and electronic contributions, $S_{Total} = S_{config} + S_{vib} + S_{mag} + S_{el}$. An increase of the degree of $L2_1$ order is expected to influence the total driving force ΔG by affecting the individual entropy contributions in S_{Total}, such as S_{vib}, S_{mag}, and S_{el}, which in turn would change $\Delta S_{tr}^{A\rightarrow M}$. The $L2_1$ ordering can even facilitate the arrest of the transformation under an applied magnetic field (with an enhanced S_{mag} contribution) or arrest the martensitic transformation without applied magnetic field (with an enhanced S_{vib} or S_{el} contribution).

Conversely, the so-called "thermal transformation arrest phenomenon" has also been explained through kinetic arguments [49,51]. For instance, it has been reported that the nucleation of the martensite phase exhibits an incubation time at low M_s temperatures in NiCoMnIn alloys [52]. The transformation habit plane in the austenite phase is believed to have restricted mobility at cryogenic temperatures as a result of the deficit in thermal energy [53]. With ample time, however, the small available thermal energy can drive the nucleation and/or propagation of martensite [54]. Therefore, the transformation is not completely arrested, but instead, transient. Additional evidence, such as increased hysteretic losses [45,49] at low temperatures and "burst-like" martensitic transformations [45] in NiCoMnIn point to a kinetic contribution to the transformation arrest. Microstructurally, isothermal behavior has been related to both nucleation and growth processes. It has been proposed that a critical martensite nuclei, estimated to be nearly 5 nm^3, would be required to match experimentally measured incubation times in an isothermal martensitic transformation for the $Ni_{45}Co_5Mn_{36.5}In_{13.5}$ MMSMA [52]. Such a microstructural feature would serve as an excellent evidence in favor of kinetic arguments that explain the transient nature of martensitic transformations. To the best of the authors' knowledge, these tiny nuclei have never been observed in arrested MMSMA.

Finally, a recent report [8] has suggested that secondary annealed NiCoMnIn MMSMAs were capable of exhibiting glass-like behaviors [55]. As mentioned earlier, these behaviors were always measured at low temperatures in a field-free environment where the martensite phase should exist, but the transformation was somehow interrupted and therefore martensite did not nucleate. It was suggested that glass-like behaviors in non-SMAs were driven by the presence of microstructural defects and that these defects should have also been present in MMSMAs exhibiting glass-like behaviors. Due to the diffusionless transformation behavior in MMSMAs, these defects are presumably locked-in the austenite phase after solution heat treatment and/or secondary annealing treatments.

1.4. Interpreting transformation arrest through microstructural observations

To shed some light on the transformation arrest in MMSMAs, we perform magneto-microstructural characterization on annealed NiCoMnIn MMSMAs. Different annealing heat treatments are shown to have a profound influence on the martensitic transformation temperatures and their decrease, which normally precedes the transformation arrest. Additionally, high-field thermomagnetic measurements are performed to probe at the thermodynamic aspects of transformation arrest in the annealed alloys. Through carefully selected heat treatments, we fully or partially suppress the martensitic transformation in a field-free conditions and perform microstructural characterization with transmission electron microscopy (TEM) in attempts to explain the effect of heat treatments on the microstructure/configuration/morphology of the

long range order within the MMSMA. Microstructural observations are compared with magnetic behaviors and lead to discussions on the microstructural origins of the transformation arrest in NiCoMnIn MMSMAs.

2. Experimental details

2.1. Material synthesis and annealing parameters

$Ni_{45}Co_5Mn_{36.6}In_{13.4}$ (at. %) MMSMAs were fabricated by vacuum induction melting of pure constituents. Single crystals were then grown via the Bridgman method under He environment. The composition of the single crystals was measured using a CAMECA SX-50 microprobe system equipped with four diffracting crystals for wavelength dispersive x-ray spectrometry (WDS). The composition was measured at multiple points in the microstructure after homogenization/solution heat treatment whereby the average measured composition was found to be $Ni_{44.9\pm0.9}Co_{5.0\pm0.1}Mn_{36.0\pm0.7}In_{14.1\pm0.3}$ at. %.

Since the NiCoMnIn single crystals exhibit drastically different martensitic transformation characteristics when annealed to promote different microstructural features [8], these treatments can be used to tune the martensitic transformation temperatures, suppress the martensitic transition, modify thermal hysteresis and transformation range, and the other properties mentioned in the introduction. Here, the starting materials were solution heat treated (SHT) at 1173 K for 24 h in high purity argon environment and then quenched in water (WQ).

The order-disorder (ODO) temperature was identified in the single crystals by employing high temperature calorimetry with a TA Instruments Q600 thermo-gravimetric analyzer (TGA). Some solution heat treated samples were furnace cooled to room temperature to maintain a high degree of diffusivity through the $L2_1$ ordering temperature on slow cooling, thereby promoting higher $L2_1$ ordering (see Fig. 2b). Next, the sample was heated during calorimetry at 20 K/min to 1300 K in an alumina pan. The $L2_1$ ordered sample exhibited an endothermic peak, corresponding to the $L2_1$ to B2 ordering temperature, around 900 K, which is close to the reported value for a similar alloy composition (896 K) [56]. Secondary annealing treatments were then performed on some single crystals above and below the ODO temperature for 3 h while encapsulated in quartz in an inert Argon atmosphere. After the secondary annealing, the samples were water quenched (WQ).

2.2. Experimental protocols

A Quantum Design superconducting quantum interference device vibrating sample magnetometer (SQUID-VSM) MPMS3 was employed to measure the thermomagnetic response of the annealed samples like those shown in Fig. 1. Sometimes, low temperature and short duration secondary annealing led to the suppression of the martensitic transformation; this was evidenced by no change in magnetization during undercooling beyond the expected M_s temperature, down to 6 K. Magnetic properties were measured by first heating the MMSMA to 400 K under zero magnetic field. At 400 K, the target field was applied (with a rate of 25 Oe/s) and then the sample was field-cooled with a rate of 5 K/min. Once the MMSMA reached the low temperature target, subsequent in-field heating was performed at 5 K/min. Thermal hysteresis ($A_f - M_s$) [57] and the austenite-to-martensite (forward) transformation temperature ranges ($M_s - M_f$) were extracted from the 0.05 T thermomagnetic data.

Differential scanning calorimetry (DSC) was also performed with a TA Instruments Q2000 DSC on the heat treated samples in a field-free condition. The resulting thermograms yielded the transformation temperatures and transformation latent heats. The samples were prepared by mechanical grinding a flat surface to maximize the thermal contact with the aluminum pan. The thermograms were then measured from 400 K to 120 K at a heating/cooling rate of 5 K/min. Before performing calorimetry on the MMSMAs, the heat capacity of a sapphire calibration standard was measured to determine a measurement correction factor. This correction factor was then applied to the MMSMA heat capacity data to minimize experimental error. The enthalpy change of the martensitic transformation was then computed from the heat flow, dQ, by

$$\Delta H_{Latent}^{A\rightarrow M} = \int_{M_f}^{M_s} \frac{dQ}{m} dT, \tag{1}$$

where m is the sample mass and the heat flow is integrated across the forward (austenite to martensite) transformation from M_s to M_f.

Furthermore, TEM was performed using an FEI Tecnai G2 microscope operated at 200 kV to identify the microstructural features responsible for the measured transformation behaviors. Single crystals were cut into 4 mm × 0.5 mm x 8 mm thin plates with electro-discharge machining (EDM). The large face of the plate was oriented perpendicular to the [011] austenite crystal direction and was verified using peak matching with a Bruker D8 X-ray diffractometer employing a Cu-K_α X-ray source tube. Plates were then annealed and mechanically ground to 100 μm thickness, punched into 3 mm diameter disks, and “twin-jet” polished using a 1:3 nitric acid to methanol electrolyte under 20 V at 243 K. Dark field images of $L2_1$ morphology were collected selecting the (111) reflection peak, using a small objective aperture, in diffraction patterns along the [011] zone axis of the austenite [58,59].

3. Results and discussions

3.1. Influence of annealing heat treatment on transformation temperatures and entropy change

Fig. 3a and b shows the measured 1 T thermomagnetic responses of the $Ni_{45}Co_5Mn_{36.6}In_{13.4}$ single crystal samples after 3 h secondary annealing treatments above and below the $L2_1$/B2 order-disorder (ODO) temperature (900 K), respectively. The samples solution heat treated (SHT) at 1173 K for 24 h (also plotted in Fig. 3a) exhibited a sharp change in magnetization at the transformation temperature, M_s, of nearly 250 K. Secondary annealing for 3 h above the ODO temperature resulted in an increase in the M_s temperature and a corresponding decrease in the magnetization change from austenite to martensite. Fluctuations in the thermal hysteresis ($A_f - M_s$) and transformation temperature ranges ($M_s - M_f$ and $A_f - A_s$) resulting from the different annealing temperatures can be clearly seen in the figure.

Interestingly, some secondary annealing heat treatments below the ODO temperature reduced M_s temperatures. As shown in Fig. 3a, the trend followed by M_s after the secondary heat treatments depends on the annealing temperature. Annealing treatments at 773 K and 873 K, both below the ODO temperature, increased the M_s temperature as compared to the SHT case, similar to the heat treatments just above the ODO temperature in Fig. 3a. On the other hand, M_s temperatures started to decrease after heat treatments at 673 K and 573 K, well below the ODO temperature. As

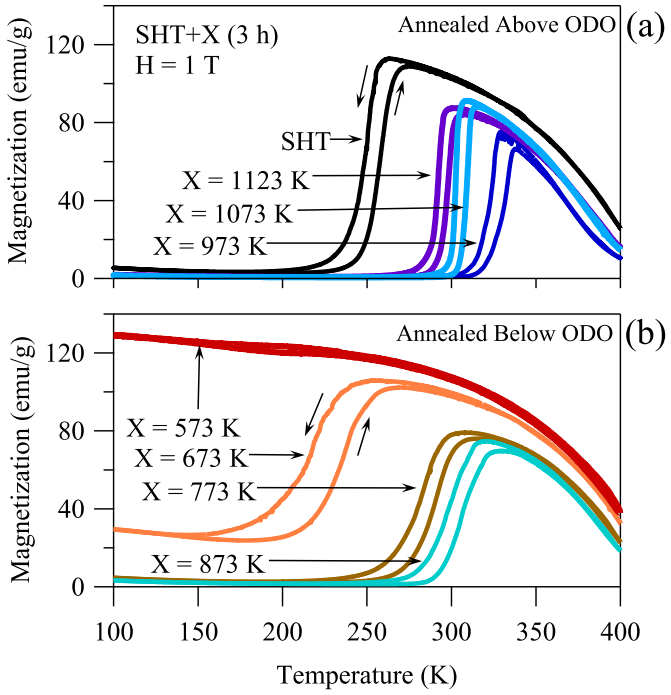

Fig. 3. The thermomagnetic responses of $Ni_{45}Co_5Mn_{36.6}In_{13.4}$ (at. %) single crystals under 1 T after 3 h annealing heat treatments above the order-disorder (ODO) temperature (a) and below the ODO temperature (b). SHT: Solution Heat Treatment.

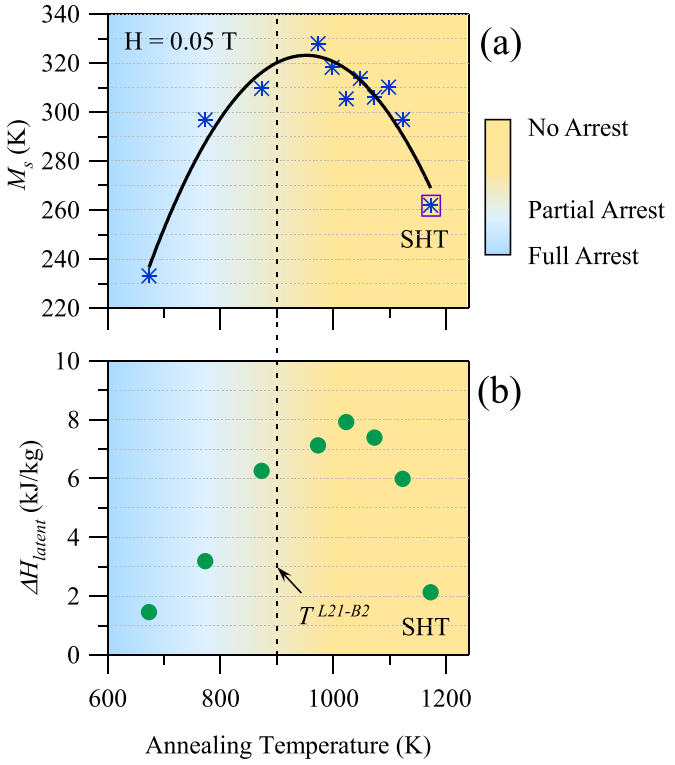

Fig. 4. The martensitic transformation start (M_s) temperature (a) and the enthalpy change of the martensitic transformation during the forward (austenite to martensite) transformation (b) as a function of the temperature of the 3 h secondary annealing. In (a), the transformation temperatures were measured from the thermomagnetic responses under 0.05 T. The SHT + 573 K (3 h) annealed alloy is omitted from the plot due to the inability to observe a clear transformation temperature. In (b), the enthalpy change was computed with Eqn. (1) described in the text. Again, SHT + 573 K (3 h) annealed alloy is omitted due to the inability to clearly observe a transformation with calorimetry. The blue background signifies the degree of transformation arrest and the $L2_1$ -B2 ordering temperature (T^{L2_1-B2}) is labeled at 900 K. (For interpretation of the references to colour in this figure legend, the reader is referred to the web version of this article.)

the M_s started to decrease, the martensitic transformation also began to exhibit very different characteristics including increased transformation temperature range, wider thermal hysteresis, and eventually suppression of the transformation, altogether, as shown by the X = 573 K curve in Fig. 3b.

The critical temperatures were extracted from the data similar to that shown in Fig. 3 and were plotted in Fig. 4a. This figure shows the M_s temperature as a function of 3 h secondary annealing temperatures. The M_s temperature of the 24 h SHT samples is also included on the same graph as an initial condition. The SHT samples exhibited a martensitic transformation at nearly 250 K and showed no apparent signs of transformation arrest. On the other hand, the samples secondary annealed at 673 K for 3 h exhibited a similar but slightly lower M_s of 230 K, and they seem to experience partial transformation arrest. Secondary annealing at temperatures between 773 K and 1173 K (SHT temperature) always increased the M_s from the SHT case by at least 40 K.

To confirm that the martensitic transformation experienced transformation arrest as a result of the low temperature annealing treatments, differential scanning calorimetry (DSC) was also performed as discussed in Section 2.2. In arrested alloys, the martensitic transformation does not progress and results in a decrease in the latent heat of the martensitic transformation. The latent heat was computed using Eqn. (1) and it would be zero for fully arrested alloys. The computed latent heats from DSC thermograms (not shown) are plotted in Fig. 4b for each 3 h secondary heat treatment. A strong correlation between the M_s temperature and the martensitic transformation latent heat can be observed. As expected, the MMSMAs secondary annealed for 3 h at 773 K exhibited a smaller transformation latent heat compared to those secondarily annealed above the ODO temperature. The exception to this is the solutionized alloy. This arrest may be the result of a reduced driving force corresponding to a specific microstructural feature that will be discussed later.

3.2. Microstructural elastic energy storage and dissipation

The forward transformation temperature range $M_s - M_f$ and thermal hysteresis $A_f - M_s$ for each 3 h secondary annealing treatment were extracted from 0.05 T thermomagnetic data and are plotted in Fig. 5. The solution heat treated alloy exhibited an $M_s - M_f$ of nearly 19 K and thermal hysteresis of 9 K. The samples with all other secondary annealing treatments above the ODO temperature showed lower transformation temperature ranges than those for the SHT alloy and approximately the same thermal hysteresis. Studies have shown that the transformation temperature range can be related to the microstructurally stored elastic energy across the martensitic transformation [9,60,61], and therefore, the secondary annealing above the ordering temperature modifies this parameter through microstructural changes.

As shown by the data in Fig. 5 below the ODO temperature, the samples with larger $M_s - M_f$ and $A_f - M_s$ ranges also exhibit relatively more transformation arrest (blue background). For data above the ODO, no apparent transformation arrest was measured, but there was a measurable variation in $M_s - M_f$ between the annealing treatments. We believe the increase in $M_s - M_f$ and $A_f - M_s$ offer clues to the microstructural conditions responsible for transformation arrest.

For instance, increased transformation temperature range in

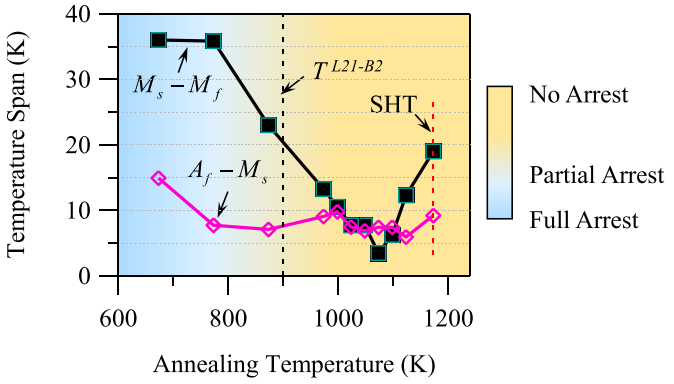

Fig. 5. The transformation temperature range ($M_s - M_f$) and the thermal hysteresis ($A_f - M_s$) as a function of the temperature of the 3 h secondary annealing treatment. The blue background signifies the degree of transformation arrest and the $L2_1$ -B2 ordering temperature (T^{L2_1-B2}) is labeled at 900 K. (For interpretation of the references to colour in this figure legend, the reader is referred to the web version of this article.)

single crystals of other SMAs after the secondary annealing could indicate the growth of nano-sized second phases [62,63], or a higher degree of microstructurally stored elastic energy through a decrease in the coherency between austenite and martensite phases in an SMA with high resistance to dislocation slip. Other effects of annealing that would modulate the transformation temperature range could include defect driven variations in the periodicity of the austenite crystal lattice, i.e. anti-site defects or vacancies.

Interestingly, regardless of the temperature of the 3 h annealing treatment above 700 K (which is notably below the ODO temperature), the thermal hysteresis was approximately constant. This suggests that B2 and $L2_1$ ordered austenite phases exhibit approximately the same dissipation through the phase transition. Only when the alloy began to exhibit transformation arrest, the dissipation through the transformation increased.

3.3. *Effects of annealing temperature and duration on microstructure and transformation arrest*

Given the above results, additional annealing treatments were performed to amplify the transformation arrest in the present single crystals. Since the transformation arrest was only observed in the samples annealed below the ODO temperature, different duration annealing treatments were performed at low temperatures intended to achieve various degrees of arrest. These annealed samples were subjected to magnetometry measurements and were studied with transmission electron microscopy in attempts to identify microstructural conditions responsible for the transformation arrest.

The single crystals were secondary annealed, after the solution heat treatment (1173 K for 24 h), at 573 K for 3 h and 168 h, 673 K for 3 h and 24 h, and 773 K for 0.25 h, 0.5 h, and 3 h. Below, we discuss the resulting measurements in detail and depict interesting behaviors related to the particular microstructure/distribution of the B2 and $L2_1$ ordered regions in the high temperature austenite phase. We show that $L2_1$ vs. B2 ordering is not the only factor contributing to the transformation arrest in MMSMAs.

Selected area electron diffraction patterns (SAEDP) obtained for the samples studied in this work always showed the fundamental spots of the B2 structure together with the superlattice reflections corresponding to the $L2_1$ structure. Thus, no perfect B2 or $L2_1$ order has been obtained either after SHT or after secondary annealing treatments; all the samples contained some amount of $L2_1$ ordered regions. Due to the dependence of the intensity of the diffracted spots to the thickness of the regions in the thin foils where the diffraction patterns were obtained, the ratio of the volume fraction between B2/$L2_1$ regions cannot be quantitatively deduced from the SAEDP. Therefore, most of the following discussion will deal with the dark field images obtained by selecting the (111)-type superlattice reflection, as explained in Section 2.2. In those images, the bright regions correspond to the zones with high volume fraction of long range $L2_1$ ordering, whereas the dark regions correspond to the zones that do not produce the (111)-type superlattice reflections (for instance, B2 ordered regions) or to antiphase boundaries. For simplicity, the non-$L2_1$ regions will be called B2 regions hereafter. It has to be also taken into account that the resulting dark field images from TEM are obtained as projections of the electrons through the entire thickness of the specimen. Therefore, in some regions, the electrons could cross $L2_1$ regions and B2 regions at different heights of the TEM specimen, producing images with different gray intensities depending on the ratio $L2_1$/B2. This can be quite common when these $L2_1$ and B2 regions are small.

The thermomagnetic response of the solution heat treated (SHT) sample is again shown in Fig. 6a. In the remaining figures, the SHT thermomagnetic curve under 1 T field will be included as a reference for comparison between the secondary annealing cases. Clearly, the SHT case does not exhibit transformation arrest as shown by a sharp decrease in magnetization at the M_s temperature (250 K) and the thermal hysteresis representative of a thermoelastic martensitic transformation.

Thermo-magnetic response for the sample annealed at 573 K for 3 h is also shown in Fig. 6a. This treatment resulted in a decrease in the transformation temperatures, which led to the partial suppression of the martensitic transformation and a slight increase in the Curie temperature of the austenite phase. Only a fraction of the material transformed to the martensite phase between M_s and M_f, as evident from the small change in the magnetization across the transformation range. A longer duration secondary annealing treatment was also performed, i.e. for 168 h at 573 K; this led to the complete suppression of the martensitic transformation as indicated by the disappearance of thermal hysteresis and no observable change in magnetization around the expected M_s temperature of 200 K. In the completely arrested sample, the saturation magnetization of the austenite phase was found to be nearly 140 emu/g and the Curie point of austenite was approximately equal to that of the 3 h annealing treatment.

The dark field micrographs obtained along the $[011]_{L2_1}$ zone axes exhibiting the $L2_1$ morphology for each annealing treatment are shown in Fig. 6b–d. The bright areas of the micrographs correspond to areas in the microstructure with a high density of $L2_1$ zones averaged through the sample thickness. In the SHT case, Fig. 6b, these areas are evenly dispersed and smaller than 20 nm. It is assumed that this sample exhibits the highest degree of B2 long range order, as it was annealed at the highest temperature and then quenched, but still it contains very small amount of $L2_1$ regions shown by dark field images and SAEDP. The state shown in Fig. 6b will be hereafter referred to by the B2 state. Secondary annealing at lower temperatures was intended to grow the $L2_1$ (bright) domains in the microstructure. Interestingly, not much change in $L2_1$ morphology was observed in the other secondary annealed alloys (Fig. 6c and d) at 573 K. The only observable difference between the micrographs in Fig. 6 is a slight coarsening of the $L2_1$ domain from lengths less than 20 nm to lengths nearly equal to 20 nm. This suggests the ordering process from B2 toward $L2_1$ occurs slowly at 573 K since the available thermal energy required for atomic diffusion is low. These images and their corresponding thermomagnetic responses indicate that either the MMSMAs are

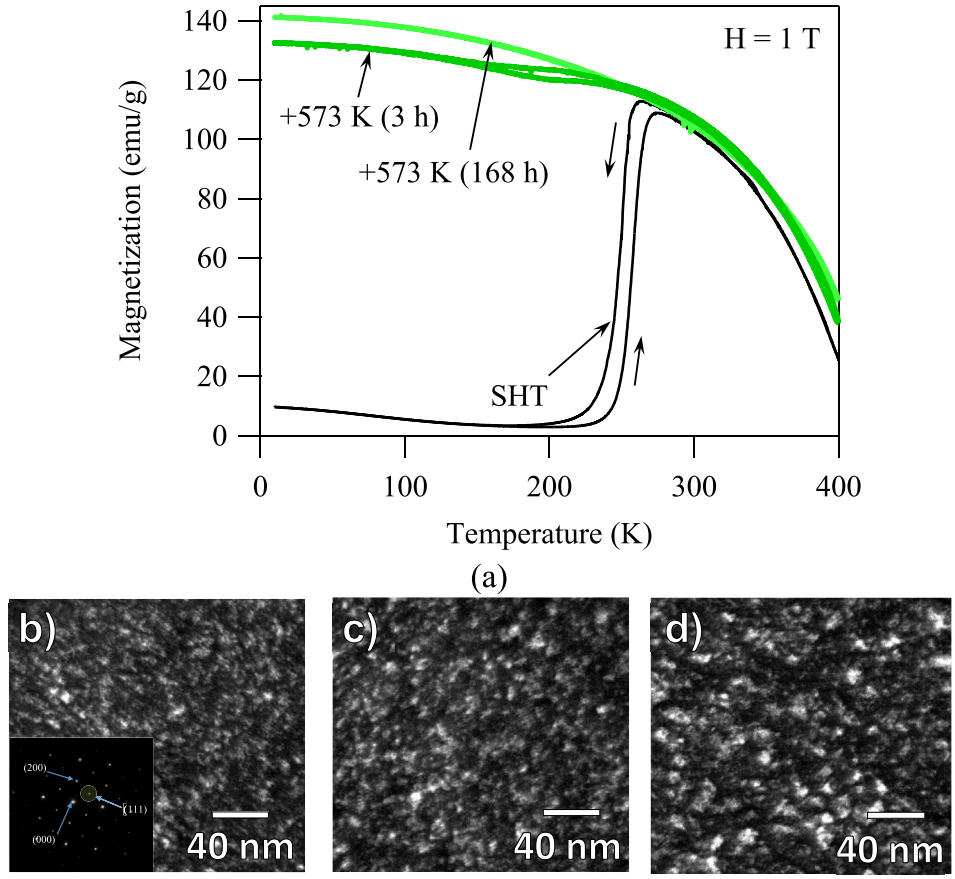

Fig. 6. The thermomagnetic responses of (a) the solution heat treated (SHT), SHT + 573 K (3 h), and SHT + 573 K (168 h) annealed $Ni_{45}Co_5Mn_{36.6}In_{13.4}$ single crystals under 1 T applied field and (b) the respective dark field images of $L2_1$ morphology for SHT, (c) SHT +573 K (3 h), and (d) SHT +573 K (168 h). Dark field micrographs were collected at room temperature using the (111) reflection peaks along the [011] austenite zone axis in the annealed single crystals.

extremely sensitive to the size of the $L2_1$ domains, or that the microstructural feature responsible for the arrest is simply not visible in the dark field micrographs. In other words, the microstructural feature that arrests the transformation might be obscured or hidden by the dark areas corresponding to the non-$L2_1$ or B2 domains.

A second set of samples was annealed at 673 K for 3 h and 24 h in an attempt to grow the $L2_1$ domains. The thermomagnetic responses for these annealed samples are compared with that of the SHT in Fig. 7a. The 3 h annealing treatment led to the partial suppression of the martensitic transformation when compared to the SHT case as indicated by a decrease in magnetization change at the martensitic transformation, slight widening of the thermal hysteresis, and a decrease in martensitic transformation temperatures. On the other hand, the martensitic transformation was completely suppressed after the 24 h secondary annealing treatment at 673 K. In all the annealing cases in Fig. 7a, the Curie temperature of the austenite phase did not exhibit significant changes. The 673 K secondary annealing treatments followed the same trend as the 573 K ones in Fig. 6a. For instance, i) 3 h annealing treatments were insufficient to completely arrest the martensitic transformation, yet the degree of suppression was notably higher at 573 K, ii) longer duration annealing treatments were able to completely arrest the transformation, and iii) the fully arrested austenite achieved similar saturation magnetization, about 140 emu/g under 1 T at 10 K.

Dark field micrographs of the $L2_1$ morphology are shown in Fig. 7b and c for the secondary annealed alloys presented in Fig. 7a. When compared to the SHT case in Fig. 6b, $L2_1$ domains had significantly coarsened with secondary annealing at 673 K. Starting from less than 20 nm in size in the SHT case, $L2_1$ domains size increased to 50 nm or larger than 100 nm after 3 h or 24 h annealing heat treatments, respectively. The $L2_1$ domain size distribution was not the only notable feature presented between annealing treatments in Fig. 7b and c. When comparing the microstructures in Fig. 7b and c, we also observed a mottled contrast within the $L2_1$ domain of the 24 h annealed sample. This mottled contrast was not seen in the $L2_1$ domains in the 3 h 673 K annealed sample.

To further probe at the mottled contrast within the $L2_1$ domains, secondary annealing treatments were performed at 773 K for 0.25 h, 0.5 h, and 3 h. Note that this annealing temperature is closer to the ODO temperature of 900 K, but still well below it. The thermomagnetic responses for each annealing case are shown in Fig. 8a. Short duration annealing treatments at 773 K led to the partial suppression of the transformation as indicated by a decrease in martensitic transformation temperatures, widening of the thermal hysteresis, the increase of the transformation temperature range and the decrease in the magnetization change upon transformation. The 0.5 h annealing at 773 K drove the martensitic transformation characteristics in a similar fashion to the 0.25 h annealed case, but to a lesser degree. On the other hand, 3 h annealing at 773 K increased the martensitic transformation temperatures from the SHT case and decreased both the magnetization change and thermal hysteresis.

The shortest duration annealing treatment at 773 K led to the highest fraction of arrested austenite at low temperatures;

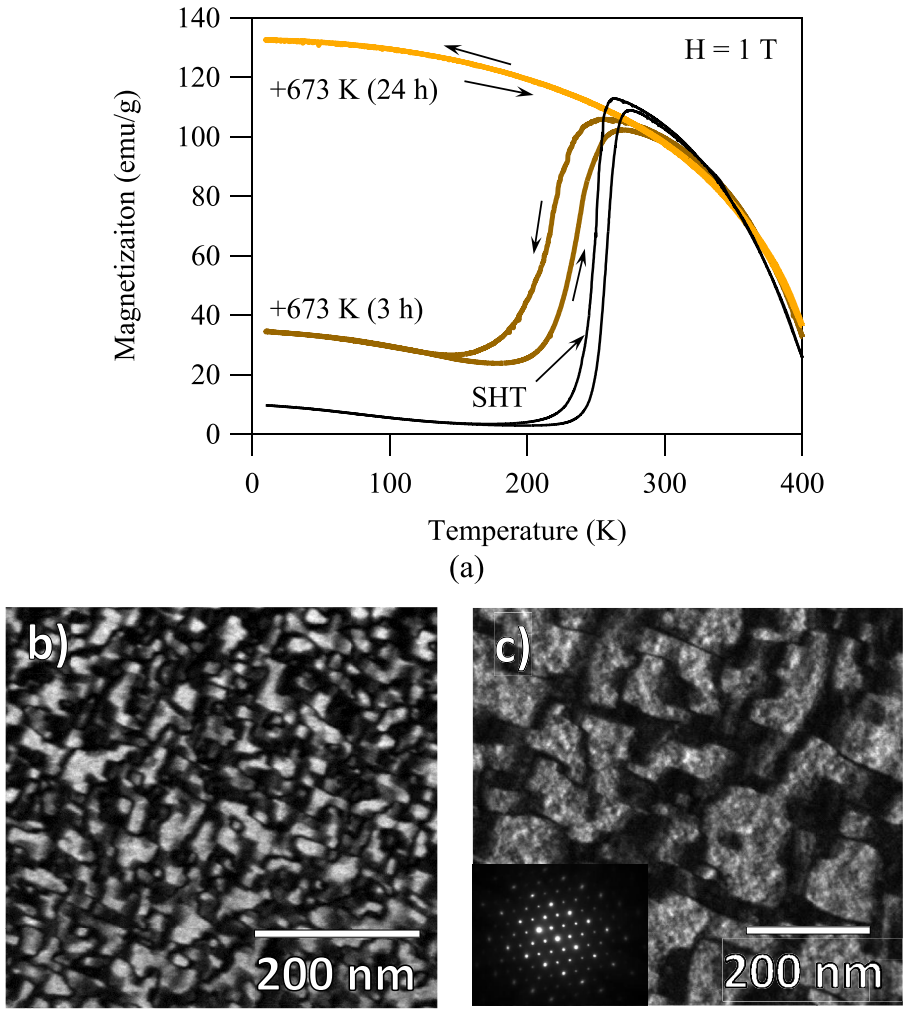

Fig. 7. The thermomagnetic responses of (a) the solution heat treated (SHT), SHT + 673 K (3 h), and SHT + 673 K (24 h) annealed $Ni_{45}Co_5Mn_{36.6}In_{13.4}$ single crystals under 1 T applied field and the respective dark field images of $L2_1$ morphology for the (b) SHT +673 K (3 h) and (c) SHT +673 K (24 h) annealing treatments. Dark field micrographs were collected at room temperature using the (111) reflection peaks along the [011] austenite zone axis in the annealed single crystals.

however, none of these heat treatments completely arrested the martensitic transformation. Therefore, the dependence of the degree of suppression on the duration of the secondary heat treatments at 773 K opposes that of the secondary heat treatments performed at 573 K or 673 K. Finally, the Curie temperature of the austenite phase was found to be approximately independent of the secondary heat treatment duration at 773 K.

Figs. 8b–d show the dark field micrographs for the 773 K secondary annealed samples. These micrographs present a clear microstructural evolution from the B2 state shown in Fig. 6b, which demonstrates the largest fraction of quenched-in B2 order, to the case in Fig. 8d exhibiting the highest volume fraction of $L2_1$ together with clear anti-phase boundaries (APBs). The micrograph in Fig. 8d corresponds to the highest degree of $L2_1$ order obtained in this work, namely the $L2_1$ state. The progression of the microstructure appeared to follow Allen-Cahn type antiphase boundary motion and domain coarsening [64]. Originally, the SHT MMSMA exhibited a disordered microstructure characterized by an even distribution of $L2_1$ domains smaller than 20 nm (Fig. 6b). Secondary annealing for 0.25 h at 773 K resulted in a diffusion driven coarsening or growth of $L2_1$ domains at the expense of the darker non-$L2_1$ microstructural areas and the formation of clear APBs. $L2_1$ domains continued to grow at the expense of the dark non-$L2_1$ domains as the annealing duration was increased to 0.5 h. At this point, domain sizes comparable to that of the 773 K 3 h annealing treatment were reached. However, the longest duration annealing treatment resulted in a nearly homogeneous $L2_1$ domain contrast absent of the mottling observed in shorter duration annealing treatments.

3.4. Interpreting the microstructure-crystallographic order-property relationships

The comparison of the observed progression of the microstructure with the measured magneto-thermoelastic response offers information never before realized for MMSMAs. For instance, past studies have demonstrated that NiCoMnIn MMSMAs exhibit an ordering temperature around 900 K and that annealing below this temperature, but at temperatures high enough for atomic diffusion to occur, would increase the volume fraction of $L2_1$ phase. The kinetics of this ordering transformation have rarely been studied [65]. Here, we have shown that $Ni_{45}Co_5Mn_{36.6}In_{13.4}$ (at. %) single crystals with a high degree of $L2_1$ long range order with distributed APBs (in Fig. 8d) exhibited higher transformation temperatures than the B2 state (Fig. 6b), having the same composition. This opposes the previous report [56] where the martensitic

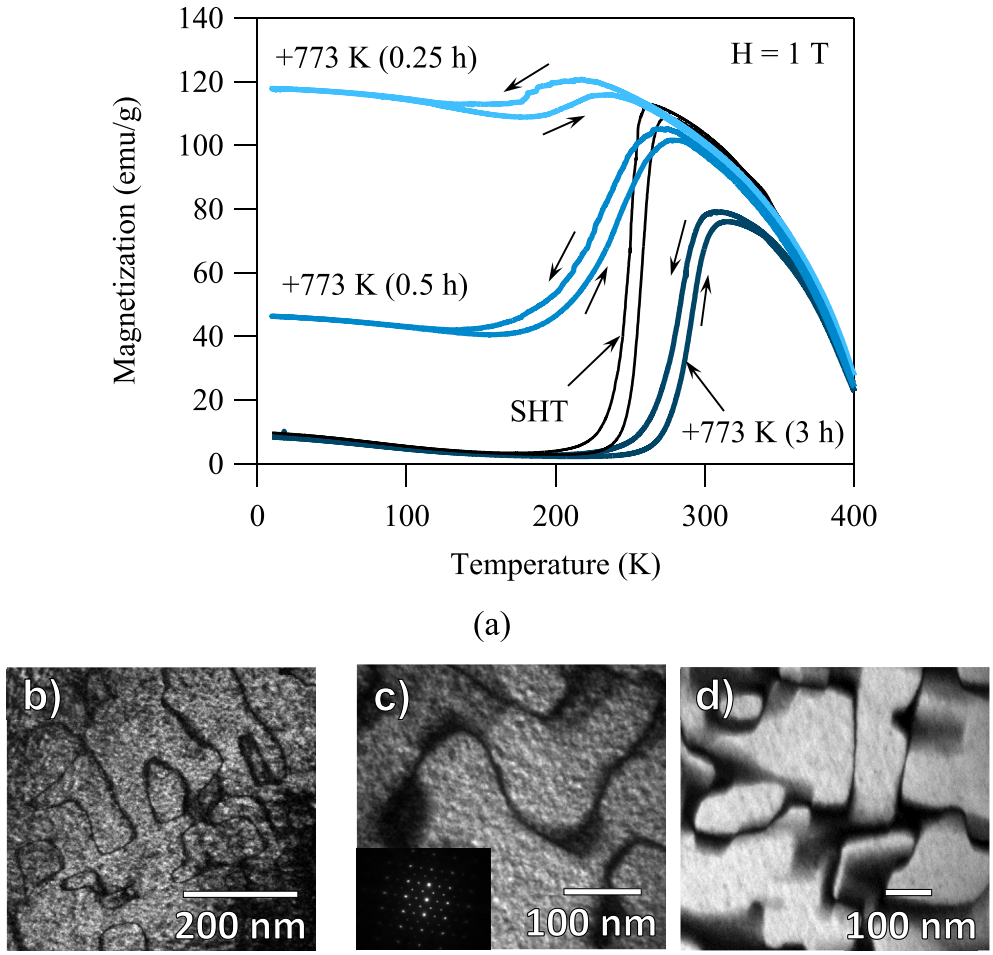

Fig. 8. The thermomagnetic responses of (a) the solution heat treated (SHT), SHT + 773 K (0.25 h), SHT + 773 K (0.5 h), and SHT + 773 K (3 h) annealed $Ni_{45}Co_5Mn_{36.6}In_{13.4}$ single crystals under 1 T applied field and the respective dark field images of $L2_1$ morphology for (b) SHT +773 K (0.25 h), (c) SHT +773 K (0.5 h), and (d) SHT +773 K (3 h) annealing treatments. Dark field micrographs were collected at room temperature using the (111) reflection peaks along the [011] austenite zone axis in the annealed single crystals.

transformation was observed at lower temperatures following secondary annealing intended to promote long range $L2_1$ ordering [8,17,18,56].

Another notable observation was that the $L2_1$ (SHT + 773 K (3 h)) and B2 (SHT) ordered microstructural states exhibited somewhat similar Curie temperatures through qualitative comparison of the thermo-magnetic responses of the austenite phases in Fig. 8. This result, again, contradicts the previous results which suggest that an increase in $L2_1$ ordering significantly increases the Curie temperature in the austenite [17,66]. Previously, the relationship between the $L2_1$ degree of atomic ordering and the arrest of the transformation has been understood through the effect of the atomic ordering on the magnetic and martensitic transformation temperatures. It was proposed that increased $L2_1$ order enhances the ferromagnetic ordering of the austenite phase and that the resulting increased magnetic contribution to the total entropy change was responsible for a measureable decline in the martensitic transformation temperatures and the total entropy change. In fact, a phenomenological inverse relationship between the transformation entropy change and the difference between the magnetic and martensitic transformation temperatures $T_c - M_s$ has been found [67–69]. In the limiting case, the transformation's chemical driving force can be completely extinguished resulting in the thermodynamic arrest of the transformation.

Enhanced ferromagnetic ordering in austenite should, then, correspond to an increase in the Curie point, however, we were unable to measure a significant increase in the Curie temperature with enhanced $L2_1$ ordering (see Fig. 8a). Here, we found that both B2 and $L2_1$ states exhibit nearly the same thermomagnetic heating/cooling response in the austenite phase. In the alloy with higher $L2_1$ order, the transformation temperatures had increased from the B2 state and the total enthalpy change of the transition was only slightly reduced (see Fig. 4b). Conversely, the low temperature or short duration annealing of the SHT alloy, that only partially promoted $L2_1$ ordering, appeared to marginally increase the Curie temperature and drastically decrease the transformation temperatures. This decrease in transformation temperatures, rather than a change in Curie temperature, appeared to be the main controlling factor for the transformation arrest.

Referring back to Fig. 4a, we observed that the SHT alloy and the 3 h secondary heat treated alloys annealed below 700 K exhibited martensitic transformation temperatures at or below 250 K. This was significant because the dark field $L2_1$ microstructures and SAEDP appeared to be nearly identical (Fig. 6b and d), however, thermomagnetic behavior under 1 T was significantly different (Fig. 6a). This demonstrates that a microstructural feature, other than the total degree of $L2_1$ ordering, is driving the martensitic transformation arrest in $Ni_{45}Co_5Mn_{36.6}In_{13.4}$ single crystals. We believe this microstructural feature is not clearly visible in dark field micrographs and that it could be related to quenched-in

vacancies generated during the solution heat treatment.

The presence of vacancies and their interaction with the ordering process may explain many of the observed behaviors, herein. For example, the SHT alloy was expected to contain the highest vacancy concentration as it had been quenched from the highest temperature. Past studies in SMAs have shown that a high vacancy concentration in the high temperature austenite phase tends to decrease the M_s temperature through lattice relaxation or a reduction in lattice stress [70,71]. This relaxation would decrease the M_s temperature through entropic stabilization of austenite [71]. A similar behavior to the one shown in Fig. 4a has been also reported in Ref. [72] for a Ni-Fe-Ga alloy and is attributed to the role of higher vacancy concentrations after thermal treatments above the ODO temperature, although no further details were presented.

On ordering the crystal lattice through secondary annealing, the M_s temperature is expected to increase with vacancy annihilation. At the same time, the M_s temperature is expected to decrease with enhanced $L2_1$ order. In this study, we measured an increase in M_s temperatures with more visible $L2_1$ ordering. Previous theoretical works have demonstrated that promoting $L2_1$ order from a B2 ordered state in Ni-based SMAs stabilizes the austenite phase and thus reduces M_s temperatures [71]. If the secondary annealing process decreases vacancy concentration and orders the crystal lattice simultaneously, non-monotonic, non-trivial behavior is expected in the M_s temperature evolution as the two processes controlling M_s are codependent.

On ordering at low temperatures through secondary annealing, we expect the high vacancy concentration from the primary annealing treatment to influence the kinetics of the ordering process. Vacancies assist atomic diffusion. Ordering, thus, should occur relatively quickly at low temperatures in a SHT sample during secondary annealing, however vacancy annihilation will occur only at vacancy sinks, such as grain boundaries or near an available interstitial atom. Since our samples are single crystalline, we believe vacancy sinks are not readily available. This interplay between vacancy annihilation (and the availability of the vacancy sinks) and the ordering should result in the non-monotonic increase/decrease of the M_s temperatures, as a function of secondary annealing temperature and time, as observed in the present work.

Finally, we posit on the thermodynamic conditions that may be responsible for the thermal transformation arrest in secondary annealed NiCoMnIn single crystals. The microstructural conditions observed through TEM suggest that some mixture of $L2_1$ and B2 ordering paired with a third unknown point defect, presumably vacancies, has the ability to arrest the martensitic transformation. Assuming our samples exhibit spatially inhomogeneous microstructures, as observed from the dark field imaging in this study, the martensite will nucleate in a heterogeneous way across a spatially dependent free energy landscape. In other words, B2 ordered microstructural regions could host martensitic nucleation, whereby the martensite then propagates across $L2_1$ ordered regions.

A spontaneous chemical reaction, or in this case an ideal martensitic transformation absent of all barriers to martensitic nucleation, can be produced if the change in Gibbs free energy, ΔG, is negative, i.e. $\Delta G = \Delta V_{tr}^{A\rightarrow M} dP - \Delta S_{tr}^{A\rightarrow M} dT - \mu_0 \Delta M_{tr}^{A\rightarrow M} dH < 0$. In an isobaric state this expression reduces to $\Delta G = -\Delta S_{tr}^{A\rightarrow M} dT - \mu_0 \Delta M_{tr}^{A\rightarrow M} dH < 0$. Here, $\Delta S_{tr}^{A\rightarrow M}$ is the entropy change across the martensitic transformation, $\Delta M_{tr}^{A\rightarrow M}$ is the change in magnetization across the transformation, T is the temperature, and H is the applied magnetic field. As mentioned earlier, the entropy term can be further reduced into components for each phase, $\Delta S_{tr}^{A\rightarrow M} = S_{Total}^{M} - S_{Total}^{A}$, where martensite and austenite exhibit their own superimposed configurational, S_{config}, vibrational, S_{vib}, magnetic, S_{mag}, and electronic, S_{el} entropies. As such, $\Delta S_{tr}^{A\rightarrow M} = \Delta S_{config}^{A\rightarrow M} + \Delta S_{vib}^{A\rightarrow M} + \Delta S_{mag}^{A\rightarrow M} + \Delta S_{el}^{A\rightarrow M}$. We believe that the vibrational, magnetic, and electronic entropy contributions play a pivotal role in transformation arrest and, therefore, their dependences on crystallographic order must be quantified to understand the arrest behavior. This is a challenging task and it will be pursued in future studies.

In the case of a field-free arrested martensitic transformation, ΔG appears to be mainly influenced by the entropy change of the system. From an ordering standpoint, a B2 ordered austenite crystal has higher configurational entropy (disorder) than $L2_1$ ordered alloys, but across the diffusionless martensitic transformation (austenite-to-martensite) this disorder is conserved. Therefore, the change in $\Delta S_{config}^{A\rightarrow M}$ with degree of crystallographic order is not expected to contribute to the arrest behavior. On the other hand, we expect that the ordering in the annealed alloys mainly influences $\Delta S_{vib}^{A\rightarrow M}$, $\Delta S_{mag}^{A\rightarrow M}$, and $\Delta S_{el}^{A\rightarrow M}$. In which case, the entropy difference between the austenite and martensite phases for these contributions may greatly depend on atomic ordering of the austenite phase.

There appears to be a non-trivial mixture of $L2_1$ and B2 ordered austenite regions that results in the transformation arrest. Since the arrest was measured in thermo-magnetic histories in MMSMAs with two completely different $L2_1$ and B2 morphologies (see Figs. 6d and 7b or 8b) we assume a third unknown and un-observed microstructural feature may also be contributing to the arrest. The long range $L2_1$ and B2 order cannot be the only factor controlling the observed transformation arrest (or interruption of the transformation) as a distinct microstructure was not observed for all cases of the arrest. The third unknown feature was not observed in our TEM micrographs and therefore, we assume the feature to be point defects including vacancies or anti-site defects that would force $\Delta G > 0$ or impose some physical barriers to martensite nucleation at low M_s temperatures. Thus, the transformation would become non-spontaneous through the interplay between $L2_1$, B2, and the un-observed microstructural features. The special "arresting" condition can be locally met with the assumptions above when $-\mu_0 \Delta M_{tr}^{A\rightarrow M} dH \geq \Delta S_{tr}^{A\rightarrow M} dT$ or $\mu_0 \Delta M_{tr}^{A\rightarrow M} / \Delta S_{tr}^{A\rightarrow M} \geq -dT/dH$. When the martensitic transformation is arrested throughout the MMSMA microstructure, martensitic nucleation appears to be thermodynamically unfavorable at all microstructural sites. In some cases where only partial transformation was observed, we expect that local microstructural conditions were favorable for spontaneous transformation, such as locally B2 ordered regions in antiphase boundaries, and therefore martensite could nucleate. However, in the inhomogeneous microstructural landscape, the propagation of the martensite was hindered.

4. Summary and conclusions

In this study, the martensitic transformation arrest phenomenon in $Ni_{45}Co_5Mn_{36.6}In_{13.4}$ MMSMA single crystals was investigated as a function of secondary annealing heat treatment temperatures and times. Dark-field TEM images of the austenite phase revealed the long range $L2_1$ and B2 ordered microstructural landscape with various different morphologies and different sizes of co-existing $L2_1$ and B2 regions. Their measured thermomagnetic responses demonstrate full transformation arrest after low temperature, long duration or medium temperature, short duration heat treatments, showing unique microstructural morphologies.

One common feature in all NiCoMnIn MMSMAs that exhibit transformation arrest is a low M_s temperature. Most studies on

NiCoMnIn attribute the reduced M_s temperatures to the long range $L2_1$ ordering. Herein, we show that the heat treatments below, but near the order-disorder (ODO) temperature that promotes $L2_1$ order from the solutionized B2 state in the $Ni_{45}Co_5Mn_{36.6}In_{13.4}$ MMSMA single crystals, is capable of increasing the M_s temperature, which is contrary to most reports. We also find that the heat treatments at considerably lower temperatures than the ODO temperature that promotes $L2_1$ order can decrease M_s. This suggests that another microstructural feature and its interaction with $L2_1$ and B2 ordering kinetics is responsible for the decrease in M_s, ultimately leading to low-temperature transformation arrest. We demonstrated that a mixture of B2 and $L2_1$ long range ordering coexisting with an unclassified defect is capable of tuning the martensitic transformation and that this microstructural defect, presumably quenched in vacancies, are responsible for the decrease in the transformation temperatures that lead to the transformation arrest behavior in $Ni_{45}Co_5Mn_{36.6}In_{13.4}$ MMSMA.

Acknowledgements

This work was supported by the U.S. National Science Foundation, Division of Materials Research, Metals and Metallic Nanostructures Program, Grant No. 1508634. Spanish MINECO and FEDER under Project Number MAT2014-56116-C4-1-R are also acknowledged for their partial financial support. R.S. acknowledges the grant by the Salvador de Madariaga Program (PRX15/00549). Y.I.C. acknowledges the support from Russian Ministry of Education and Science project 16.6554.2017/6.7 and from The Tomsk State University Academic D.I. Fund Program project 8.140.2017.

References

[1] H.E. Karaca, I. Karaman, B. Basaran, Y. Ren, Y.I. Chumlyakov, H.J. Maier, Magnetic field-induced phase transformation in NiMnCoIn magnetic shape-memory alloys – a new actuation mechanism with large work output, Adv. Funct. Mater. 19 (2009) 983.
[2] Y. Song, K.P. Bhatti, V. Srivastava, C. Leighton, R.D. James, Thermodynamics of energy conversion via first order phase transformation in low hysteresis magnetic materials, Energy Environ. Sci. 6 (2013) 1315.
[3] B. Emre, N.M. Bruno, S. Yuce, I. Karaman, Effect of niobium addition on the martensitic transformation and magnetocaloric effect in low hysteresis NiCoMnSn metamagnetic shape memory alloys, Appl. Phys. Lett. 105 (2014) 23190.
[4] I. Karaman, H.E. Karaca, B. Basaran, D.C. Lagoudas, Y.I. Chumlyakov, H.J. Maier, Stress-assisted reversible magnetic field-induced phase transformation in Ni_2MnGa magnetic shape memory alloys, Scr. Mater. 55 (2006) 403.
[5] N.M. Bruno, I. Karaman, J.H. Ross Jr., Y.I. Chumlyakov, High-field magneto-thermo-mechanical testing system for characterizing multiferroic bulk alloys, Rev. Sci. Inst. 86 (2015) 113902.
[6] J.A. Monroe, I. Karaman, B. Basaran, W. Ito, R.Y. Umetsu, R. Kainuma, K. Koyama, Y.I. Chumlyakov, Direct measurement of large reversible magnetic-field-induced strain in Ni-Co-Mn-In metamagnetic shape memory alloys, Acta Mater. 60 (2012) 6883.
[7] H.E. Karaca, I. Karaman, B. Basaran, D.C. Lagoudas, Y.I. Chumlyakov, H.J. Maier, On the stress-assisted magnetic-field-induced phase transformation in Ni_2MnGa ferromagnetic shape memory alloys, Acta Mater. 55 (2007) 4253.
[8] J.A. Monroe, J.E. Raymond, X. Xu, M. Nagasako, R. Kainuma, Y.I. Chumlyakov, R. Arroyave, I. Karaman, Multiple ferroic glasses via ordering, Acta Mater. 101 (2015) 107.
[9] N.M. Bruno, Y.J. Huang, C.L. Dennis, J.G. Li, R.D. Shull, J.H. Ross Jr., Y.I. Chumlyakov, I. Karaman, Effect of grain constraint on the field requirements for magnetocaloric effect in $Ni_{45}Co_5Mn_{40}Sn_{10}$ melt-spun ribbons, J. Appl. Phys. 120 (2016) 075101.
[10] N.M. Bruno, C. Yegin, I. Karaman, J.-H. Chen, J.H. Ross Jr., J. Liu, J. Li, The effect of heat treatments on $Ni_{43}Mn_{42}Co_4Sn_{11}$ meta-magnetic shape memory alloys for magnetic refrigeration, Acta Mater. 74 (2014) 66.
[11] N.M. Bruno, I. Karaman, J.H. Ross Jr., Y.J. Huang, J.G. Li, The tunable microstructure and its influence on the giant magnetocaloric effect in magnetic shape memory alloys, in TMS Middle East - Mediterranean Materials Congress on Energy and Infrastructure Systems (MEMA 2015) (eds I.Karaman, R.Arróyave and E.Masad), John Wiley & Sons, Inc., Hoboken, NJ, USA.
[12] T.D. Brown, N.M. Bruno, J.H. Chen, I. Karaman, J.H. Ross Jr., P.J. Shamberger, A preisach-based nonequilibrium methodology for simulating performance of hysteretic magnetic refrigeration cycles, JOM 67 (2015) 2123.
[13] S. Ozdemir Kart, M. Uludogan, I. Karaman, T. Cagin, DFT studies on structure, mechanics and phase behavior of magnetic shape memory alloys: Ni_2MnGa, Phys. Status Solidi A 205 (2008) 1026.
[14] R. Kainuma, Y. Imano, W. Ito, Y. Sutou, H. Morito, S. Okamoto, O. Kitakami, K. Oikawa, A. Fujita, T. Kanomata, K. Ishida, Magnetic-field-induced shape recovery by reverse phase transformation, Nature 439 (2006) 957.
[15] H. Funakubo, Shape Memory Alloys, Taylor & Francis, 1987.
[16] N.M. Bruno, The Magnetocaloric and Elastocaloric Effects in Magnetic Shape Memory Alloys, Ph. D. Dissertation, Texas A&M University, 2015.
[17] V. Sanchez-Alarcos, V. Recarte, J.I. Perez-Landazabal, E. Cesari, J.A. Rodriguez-Velamazan, Long-range atomic order and entropy change at the martensitic transformation in a Ni-Mn-In-Co metamagnetic shape memory alloy, Entropy 16 (2014) 2756.
[18] V. Recarte, J.I. Perez-Landazabal, V. Sanchez-Alarcos, J.A. Rodriguez-Velamazan, Dependence of the martensitic transformation and magnetic transition on the atomic order in Ni-Mn-In metamagnetic shape memory alloys, Acta Mater. 60 (2012) 1937.
[19] T. Krenke, E. Duman, M. Acet, E.F. Wassermann, X. Moya, L. Manosa, A. Planes, Inverse magnetocaloric effect in ferromagnetic Ni-Mn-Sn Alloys, Nat. Mater. 4 (2005) 450.
[20] K. Ullakko, J.K. Huang, C. Kantner, R.C. O'Handley, V.V. Kokorin, Large magnetic-field-induced strains in Ni_2MnGa single crystals, Appl. Phys. Lett. 69 (1996) 1966.
[21] P. Mullner, V.A. Chernenko, G. Kostorz, Stress-induced twin rearrangement resulting in change of magnetization in a Ni-Mn-Ga ferromagnetic martensite, Scr. Mater. 49 (2003) 129.
[22] P. Mullner, V.A. Chernenko, G. Kostorz, Large cyclic magnetic-field-induced deformation in orthorhombic (14M) Ni-Mn-Ga martensite, J. Appl. Phys. 95 (2004) 1531.
[23] I. Karaman, B. Basaran, H.E. Karaca, A.I. Karsilayan, Y.I. Chumlyakov, Energy Harvesting using martensite variant reorientation Mechanism in NiMnGa magnetic shape memory alloy, Appl. Phys. Lett. 90 (2007) 172505.
[24] H.E. Karaca, I. Karaman, B. Basaran, Y.I. Chumlyakov, H.J. Maier, Magnetic field and stress induced martensite reorientation in NiMnGa ferromagnetic shape memory alloy single crystals, Acta Mater. 54 (2006) 233.
[25] A. Sozinov, A.A. Likhachev, N. Lanska, K. Ullakko, Giant magnetic-field-induced strain in NiMnGa seven-layered martensitic phase, Appl. Phys. Lett. 80 (2002) 1746.
[26] T. Kihara, X. Xu, W. Ito, R. Kainuma, M. Tokunaga, Direct measurements of inverse magnetocaloric effects in metamagnetic shape-memory alloy NiCoMnIn, Phys. Rev. B 90 (2014) 214409.
[27] H.E. Karaca, I. Karaman, A. Brewer, B. Basaran, Y.I. Chumlyakov, H.J. Maier, Shape memory and pseudoelasticity response of NiMnCoIn magnetic shape memory alloy single crystals, Scr. Mater. 58 (2008) 815.
[28] B.M. Wang, Y. Liu, L. Wang, S.L. Huang, Y. Zhao, Y. Yang, H. Zhang, Exchange bias and its training effect in the martensitic state of bulk polycrystalline $Ni_{49.5}Mn_{34.5}In_{16}$, J. Appl. Phys. 104 (2008) 043916.
[29] B.M. Wang, Y. Liu, P. Ren, B. Xia, K.B. Ruan, J.B. Yi, J. Ding, X.G. Li, L. Wang, Large exchange bias after zero-field cooling from an unmagnetized state, Phys. Rev. Lett. 106 (2011) 077203.
[30] B.M. Wang, P. Ren, Y. Liu, L. Wang, Enhanced magnetoresistance through magnetic-field-induced phase transition in Ni_2MnGa co-doped with Co and Mn, J. Magn. Magn. Mater. 322 (2010) 715.
[31] V.K. Sharma, M.K. Chattopadhyay, S.K. Nath, K.J. Sokhey, R. Kumar, P. Tiwari, S.B. Roy, The effect of substitution of Mn by Fe and Cr on the martensitic transition in the $Ni_{50}Mn_{34}In_{16}$ alloy, J. Phys. Condens. Mat. 22 (2010) 486007.
[32] Y. Wang, C. Huang, J. Gao, S. Yang, X. Ding, X. Song, X. Ren, Evidence for ferromagnetic strain glass in Ni-Co-Mn-Ga Heusler alloy system, Appl. Phys. Lett. 101 (2012) 101913.
[33] W. Zhigang, Strain Glass behavior of Ni-Co-Mn-Sn ferromagnetic shape memory alloys, Phys. Status Solidi RRL 9 (2015) 317.
[34] X. Ren, Strain glass and ferroic glass – unusual properties from glassy nanodomains, Phys. Status Solidi B 251 (2014) 1982.
[35] X.Y. Yu, Z.X. Cao, L. Ma, G.D. Liu, J.L. Chen, G.H. Wu, B. Zhang, X.X. Zhang, Realization of magnetic field-induced reversible martensitic transformation in NiCoMnGa alloys, Appl. Phys. Lett. 91 (2007) 102507.
[36] W. Ito, Y. Imano, R. Kainuma, Y. Sutou, K. Oikawa, K. Ishida, Martensitic and magnetic transformation behaviors in Heusler-type NiMnIn and NiCoMnIn metamagnetic shape memory alloys, Metall. Mater. Trans. A 38A (2007) 759.
[37] E. Sasioglu, L.M. Sandratskii, P. Bruno, Role of conduction electrons in mediating exchange interactions in Mn-based Heusler alloys, Phys. Rev. B 77 (2008) 064417.
[38] T. Graf, C. Felser, S.S.P. Parkin, Simple rules for the understanding of Heusler compounds, Prog. Solid State Chem. 39 (2011) 1.
[39] H. Yang, Y. Chen, H. Bei, C.R. dela Cruz, Y.D. Wang, K. An, Annealing effects on the structural and magnetic properties of off-stoichiometric Fe-Mn-Ga ferromagnetic shape memory alloys, Mater. Des. 104 (2016) 327.
[40] C. Yegin, Magneto-thermo-mechanical Response and Magneto-caloric Effect in Magnetic Shape Memory Alloys, Master Thesis, Texas A&M University, 2012.
[41] J. Pons, E. Cesari, C. Segui, F. Masdeu, R. Santamarta, Ferromagnetic shape memory alloys: alternatives to Ni-Mn-Ga, Mater. Sci. Eng. A 481–482 (2007) 57.
[42] N.M. Bruno, Energy Harvesting Using Martensitic Variant Reorientation in $Ni_{50}Mn_{28.5}Ga_{21.5}$ Magnetic Shape Memory Alloy, Master Thesis, Northern Arizona University, 2011.

[43] B. Kiefer, D.C. Lagoudas, Magnetic field-induced martensitic variant reorientation in magnetic shape memory alloys, Philos. Mag. 85 (2005) 4289.
[44] S. Yuce, N.M. Bruno, B. Emre, I. Karaman, Accessibility investigation of large magnetic entropy change in $CoMn_{1-x}Fe_xGe$, J. Appl. Phys. 119 (2016) 133901.
[45] W. Ito, K. Ito, R.Y. Umetsu, R. Kainuma, K. Koyama, K. Watanabe, A. Fujita, K. Oikawa, K. Ishida, T. Kanomata, Kinetic Arrest of martensitic transformation in the NiCoMnIn metamagnetic shape memory alloy, Appl. Phys. Lett. 92 (2008) 021908.
[46] R.Y. Umetsu, X. Xu, R. Kainuma, NiMn-based metamagnetic shape memory alloys, Scr. Mater. 116 (2016) 1–6.
[47] P.J. Stonaha, M.E. Manley, N.M. Bruno, I. Karaman, R. Arroyave, N. Singh, D.L. Abernathy, S. Chi, Lattice vibrations boost demagnetization entropy in a shape-memory alloy, Phys. Rev. B 92 (2015) 140406(R).
[48] A. Planes, L. Mañosa, E. Vives, J. Rodriguez-Carvajal, M. Morin, G. Guenin, J.L. Macqueron, Neutron diffraction study of long-range atomic order in Cu-Zn-Al shape memory alloys, J. Phys. Condens. Mat. 4 (1992) 553.
[49] R.Y. Umetsu, X. Xu, W. Ito, T. Kihara, K. Takahashi, M. Tokunaga, R. Kainuma, Magnetic field-induced reverse martensitic transformation and thermal transformation arrest phenomenon of $Ni_{41}Co_9Mn_{39}Sb_{11}$ alloy, Metals 4 (2014) 609–622.
[50] X. Xu, W. Ito, M. Tokunaga, T. Kihara, K. Oka, R.Y. Umetsu, T. Kanomata, R. Kainuma, The thermal transformation arrest phenomenon in NiCoMnAl Heusler Alloys, Metals 3 (2013) 298.
[51] X. Xu, W. Ito, R.Y. Umetsu, R. Kainuma, K. Ishida, Anomaly of critical stress in stress-induced transformation of NiCoMnIn metamagnetic shape memory alloy, Appl. Phys. Lett. 95 (2009) 181905.
[52] T. Fukuda, T. Kakeshita, Y. Lee, An interpretation of the kinetics of martensitic transformation in a $Ni_{45}Co_5Mn_{36.5}In_{13.4}$ alloy, Acta Mater. 81 (2014) 121.
[53] R.Y. Umetsu, W. Ito, K. Ito, K. Koyama, A. Fujita, K. Oikawa, T. Kanomata, R. Kainuma, K. Ishida, Anomaly in entropy change between parent and martensite phases in the $Ni_{50}Mn_{34}In_{16}$ Heusler alloy, Scr. Mater. 60 (2009) 25–28.
[54] J.I. Perez-Landazabal, V. Recarte, V. Sanchez-Alarcos, S. Kustov, D. Salas, E. Cesari, Effect of magnetic field on the isothermal transformation of a Ni-Mn-In-Co magnetic shape memory alloy, Intermetallics 28 (2012) 144–148.
[55] V.K. Sharma, M.K. Chattopadhyay, S.B. Roy, Kinetic Arrest of the first-order austenite to martensite phase transition in $Ni_{50}Mn_{34}In_{16}$: dc magnetization studies, Phys. Rev. B 76 (2007) 140401.
[56] W. Ito, M. Nagasako, R.Y. Umetsu, R. Kainuma, T. Kanomata, K. Ishida, Atomic ordering and magnetic properties in the $Ni_{45}Co_5Mn_{36.7}In_{13.3}$ metamagnetic shape memory alloy, Appl. Phys. Lett. 93 (2008) 232503.
[57] H.C. Tong, C.M. Wayman, Characteristic temperatures and other properties of thermoelastic martensites, Acta Metall. 22 (1976) 887.
[58] Y. Murakami, D. Shindo, K. Kobayashi, K. Oikawa, R. Kainuma, K. Ishida, TEM studies of crystallographic and magnetic microstructures in Ni-based ferromagnetic shape memory alloys, Mater. Sci. Eng. A 438–440 (2006) 1050.
[59] Y. Murakami, K. Yanagisawa, K. Niitsu, H.S. Park, T. Matsuda, R. Kainuma, D. Shindo, A. Tonomura, Determination of magnetic flux density at the nanometer-scale antiphase boundary in Heusler alloy $Ni_{50}Mn_{25}Al_{12.5}Ga_{12.5}$, Acta Mater. 61 (2013) 2095.
[60] P. Wollants, J.R. Roos, L. Delaey, Thermally- and stress-induced thermoelastic martensitic transformations in the reference frame of equilibrium thermodynamics, Prog. Mater. Sci. 37 (1993) 227.
[61] M. Ahlers, R. Pascual, R. Rapacioli, W. Arneodo, Transformation hardening and energy-dissipation in martensitic beta-brass, Mater. Sci. Eng. 27 (1977) 49.
[62] R. Santamarta, A. Evirgen, A.M. Perez-Sierra, J. Pons, E. Cesari, I. Karaman, R.D. Noebe, Effect of thermal treatments on Ni-Mn-Ga and Ni-Rich Ni-Ti-Hf/Zr high-temperature shape memory alloys, Shape Mem. Superelas. 1 (2015) 418.
[63] I.V. Kireeva, C. Cicornell, J. Pons, I.V. Kretinina, Y.I. Chumlyakov, E. Cesari, Effect of oriented γ' precipitates on shape memory effect and superelasticity in Co-Ni-Ga single crystals, Acta Mater. 68 (2014) 127.
[64] S.M. Allen, J.W. Cahn, Microscopic theory for antiphase boundary motion and its application to antiphase domain coarsening, Acta Metall. Mater. 27 (1979) 1085.
[65] R.W. Overholser, M. Wuttig, Chemical ordering in NiMnGa Heusler alloys, Scr. Mater. 40 (1999) 1095.
[66] P. Neibecker, M. Leitner, G. Benka, W. Petry, Increasing the achievable state of order in Ni-based Heusler alloys via quenched-in vacancies, Appl. Phys. Lett. 105 (2014) 261904.
[67] E. Cesari, D. Salas, S. Kustov, Entropy changes in ferromagnetic shape memory alloys, Mater. Sci. Forum 684 (2011) 49.
[68] A.M. Perez-Sierra, N.M. Bruno, J. Pons, E. Cesari, I. Karaman, Atomic order and martensitic transformation entropy change in Ni-Co-Mn-In metamagnetic shape memory alloys, Scr. Mater. 110 (2016) 61.
[69] V. Recarte, J.I. Perez-Landazabal, V. Sanchez-Alarcos, V. Zablotskii, E. Cesari, S. Kustov, Entropy change linked to the martensitic transformation in metamagnetic shape memory alloys, Acta Mater. 60 (2012) 3168.
[70] A.M. Tehrani, H. Shahrokhshahi, N. Parvin, J. Brgoch, Influencing the martensitic phase transformation in NiTi through point defects, J. Appl. Phys. 118 (2015) 014901.
[71] T.Y. Hsu, Y. Linfah, The effect of quenched-in vacancies on the martensitic transformation, J. Mater. Sci. 18 (1983) 3213.
[72] R. Santamarta, E. Cesari, J. Font, J. Muntasell, J. Pons, J. Dutkiewicz, Effect of atomic order on the martensitic transformation of Ni-Fe-Ga alloys, Scr. Mater. 54 (2006) 1985.